

Self-referenced nonlinear interferometry for chromatic dispersion sensing across multiple length scales

Romain Dalidet, Sébastien Tanzilli, Gregory Sauder, Laurent Labonté* and Anthony Martin
Université Côte d'Azur, CNRS, Institut de physique de Nice, France

Chromatic dispersion critically impacts the performance of numerous applications ranging from telecommunication links to ultrafast optics and nonlinear devices, yet fast and precise measurements are challenging, especially for short length-dispersion products. We present a fully fiber-integrated nonlinear Sagnac interferometer that exploits cascaded second-order processes to generate frequency- anticorrelated idler light and achieve odd-order dispersion cancellation without active stabilization. The measurement is intrinsically self-referenced, as the dispersion-induced phase is extracted from the interference between counter-propagating nonlinear processes within the same Sagnac loop, eliminating the need for an external reference arm or prior calibration. Operating entirely at telecom wavelengths and read out on a standard optical spectrum analyzer, the device produces instantaneous, high-visibility fringes and calibration-free spectra using dual-port normalization. We demonstrate chromatic dispersion measurements on fiber samples ranging from 25 cm to 4 km, spanning short fiber segments to long-haul links. This architecture combines self-stability, broadband compatibility, and rapid acquisition, offering a practical metrology tool for both research and industry.

I. INTRODUCTION

Optical phase estimation is a cornerstone of both classical and quantum metrology, enabling high-performance measurements in fields as diverse as gravitational-wave detection [1], optical coherence tomography [2], displacement sensing [3], and gyroscopy [4]. In applied photonics, it underpins the characterization of waveguide dispersion [6, 20] and the development of integrated photonic circuits [7].

Accurate chromatic dispersion (CD) measurements are particularly challenging when the length-dispersion product of the sample is small, as in the case of short fibers, integrated photonic devices, or specialty components. Conventional phase-shift or modulation-based techniques [6, 8] lose sensitivity in this regime, whereas classical white-light interferometry requires precise wavelength balancing [9]. In industrial metrology, there is a growing demand for methods that combine broadband coverage, high precision, and short acquisition times without the complexity of environmental isolation or free-space alignment.

Classical interferometers such as Mach-Zehnder and Michelson designs are widely used for precision phase sensing, but they are highly sensitive to environmental fluctuations and typically require active stabilization [9]. Nonlinear interferometers, including SU(1,1) configurations [10, 11] and quantum-induced-coherence architectures [12–14], have been applied to CD measurement [15, 16], offering intrinsic odd-order dispersion cancellation [17] and relaxed path-length stability requirements. However, many implementations require the sample under test to be transparent at two wavelengths, which often limits the experiment to bulk optics and alignment

sensitive setups. More generally, quantum-probe operations, such as two-photon interference, rely on narrow-band filtering and single-photon detection, resulting in long acquisition times.

Here, we introduce a fully fibered, self-referenced nonlinear interferometer based on cascaded second-order processes in a Sagnac loop to accurately measure the CD. This design achieves self-stabilization [18] and odd-order dispersion cancellation while operating entirely at telecom wavelengths. This architecture allows direct broadband readout on a standard optical spectrum analyzer, enabling fast, calibration-free measurements from short to long fiber samples, effectively filling a gap in interferometric sensing and meeting the needs of industrial metrology.

II. METHODS

The dispersion of an optical material, or equivalently, the relative spectral phase in an interferometer, is commonly expressed as a Taylor expansion of the wave vector around the central frequency ω_0 of the light propagating through it:

$$k(\omega) = \sum_{n=0}^{\infty} \frac{\partial^n k}{\partial \omega^n} \bigg|_{\omega_0} \frac{(\omega - \omega_0)^n}{n!} = \sum_{n=0}^{\infty} \beta^{(n)} \frac{\Delta\omega^n}{n!}. \quad (1)$$

Here, the second-order term $\beta^{(2)}$ corresponds to the chromatic dispersion. Because the hierarchy $\beta^{(n)} \gg \beta^{(n+1)}$ generally holds for optical materials, interferometric extraction of the CD in the frequency (or time) domain requires the cancellation of the first-order term $\beta^{(1)}$ (group delay) in the interferometer's relative phase. In white-light interferometry, this is achieved by balancing the interferometer at the stationary-phase point so that the relative spectral phase becomes independent of $\beta^{(1)}$. In quantum white-light (QWLI) interferometry based on

* laurent.labonte@univ-cotedazur.fr

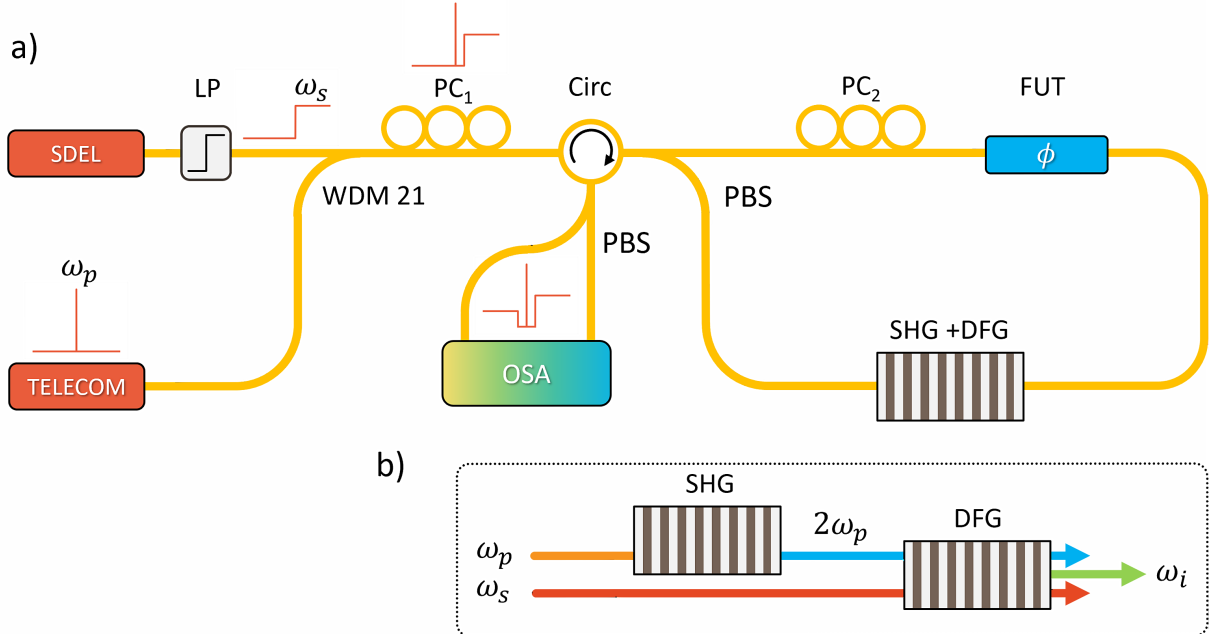


FIG. 1. a) Experimental setup for CD measurement using a cascaded nonlinear Sagnac interferometer. A Superluminescent diode and pump laser generate a frequency-anticorrelated superposed state inside the loop via a nonlinear crystal. The CD of the FUT is retrieved by measuring the interference fringes on a standard OSA. b) Schematic of the cascaded nonlinear process. The pump is first converted into its second harmonic, which then interacts with the signal in the second step to generate an idler via difference-frequency generation. SDEL : superluminescent diode. WDM: Wavelength-division multiplexer. PC: Polarization controller. Circ: circulator. PBS: Polarizing beam splitter. FUT : fiber under test. SHG: Second-harmonic generation. DFG: difference-frequency generation. OSA: optical spectrum analyzer.

energy-correlated photon pairs, energy and phase conservation impose that the total phase is the sum of the individual phases; under these constraints, all odd-order dispersion terms cancel in the relative phase (nonlocal dispersion cancellation) [17]. Importantly, although this cancellation was originally interpreted as a nonlocal quantum effect, the suppression of odd-order dispersion terms is, from a local perspective, a direct consequence of energy and phase conservation during the nonlinear generation process [19]. This local interpretation forms the basis of our experimental approach, as illustrated in Fig. 1(a), respectively.

A telecom laser centered at $\lambda_p = 1560.6$ nm and a superluminescent diode (SDEL) filtered in the L-band using a long-pass filter (LP) are used as pump sources. The frequency of the filtered SDEL, denoted ω_s , defines the signal beam. Both the pump and signal are combined via a wavelength division multiplexer (WDM) and transmitted through a polarization controller PC₁ and a circulator. The first output port of the circulator feeds a nonlinear Sagnac interferometer composed of a polarizing beam splitter (PBS), second PC, fiber under test (FUT), and polarization-maintaining nonlinear crystal (MgO-doped LiNbO₃) engineered for second-order nonlinear interactions. We emphasize that both outputs of the PBS are aligned along the same axis and that all fibers, including those of the crystal, are PM fibres. Therefore, if the

FUT is also a PM, the entire Sagnac loop preserves the polarization, and the PC inside the loop can be removed.

First, we describe the cascaded nonlinear interaction in the crystal, as shown schematically in Fig. 1(b). For simplicity, we considered a process occurring in two identical nonlinear crystals. The first crystal, pumped by the telecom laser, performs second-harmonic generation (SHG) at a frequency $2\omega_p$. The second crystal, pumped by this SHG beam and signal ω_s , performs difference-frequency generation (DFG), producing an idler at frequency ω_i satisfying

$$\omega_i = 2\omega_p - \omega_s , \quad (2)$$

$$k_i = 2k_p - k_s . \quad (3)$$

A factor of 2 in these expressions arises from the SHG process, whereas the minus sign corresponds to the DFG step. Thus, the idler is energy-anticorrelated with the signal, centered around the pump frequency ω_p . In our experiment, both SHG and DFG occur in the same crystal designed for operation in the C+L band, which is phase-matched at $2\omega_p$, and the poling period and phase-matching temperature are identical for both nonlinear steps. Because the SHG beam is only an intermediate, it is not collected; the pigtailed of the crystal are optimized for telecom wavelengths to maximize the coupling and collection of the pump, signal, and idler beams.

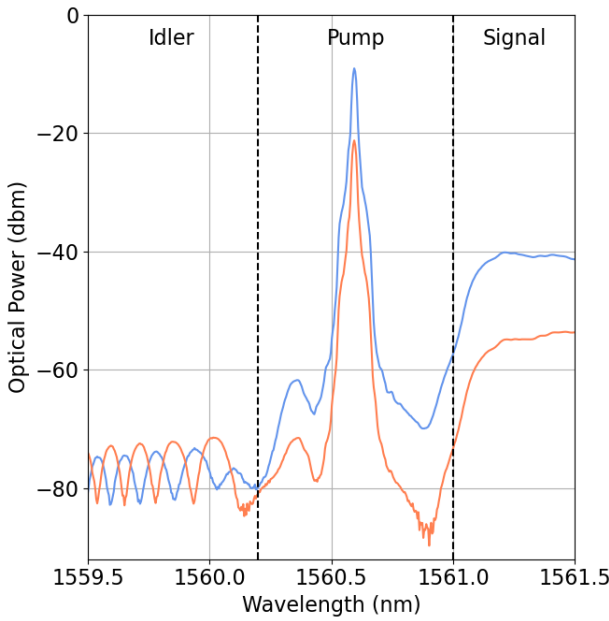


FIG. 2. Raw spectra measured by the optical spectrum analyzer at the two output ports of the final PBS in the setup. The complementary spectral modulations in the idler part arise from the interference and confirm the high visibility and intrinsic stability of the Sagnac configuration.

We now turn our attention to the interferometric configuration. The Sagnac loop provides intrinsic phase stability, for any external perturbations, for example thermal or mechanical, evolving on time scales much slower than the loop round-trip, the relative phase between clockwise (CW) and counterclockwise (CCW) paths remains zero. In the absence of rotation, both paths are equal in length, relaxing the usual coherence time constraints on the pump sources. This self-referencing property explains the widespread use of Sagnac interferometers to probe non-reciprocal phase shifts, such as those induced by the Faraday or Sagnac effects. To measure chromatic dispersion while preserving phase stability, the interferometer must contain a non-reciprocal element that encodes the sample dispersion differently in the two directions. In this case, the nonlinear crystal fulfills this role. By preparing both the pump and signal beams in a diagonal polarization state at the loop entrance, we generate a balanced superposition of CW and CCW paths. In the CW arm, the pump and signal propagate through the FUT before entering the crystal, whereas in the CCW arm, the nonlinear interaction occurs first, and the idler then propagates through the FUT. This asymmetry produces a non-reciprocal spectral phase difference.

As previously stated, in the CW arm, the pump and signal pass through the FUT before entering the crystal and generating an idler. The resulting phase is:

$$\phi_{\text{CW}} = (2k_p - k_s)L, \quad (4)$$

where L denotes the length of the FUT. In the CCW arm, a nonlinear interaction occurs first, generating the idler, which then propagates through the FUT:

$$\phi_{\text{CCW}} = k_i L. \quad (5)$$

The resulting non-reciprocal relative phase is therefore

$$\begin{aligned} \Phi &= \phi_{\text{CW}} - \phi_{\text{CCW}} \\ &= (2k_p - k_s - k_i)L. \end{aligned} \quad (6)$$

Using energy conservation for the cascaded SHG–DFG process, the frequency detuning of the signal and idler are anticorrelated $\Delta\omega_s = -\Delta\omega_i = \Delta\omega$. Substituting Eq. 1 into Eq. 6 yields:

$$\Phi = \beta^{(2)} L \Delta\omega^2 + \mathcal{O}(\Delta\omega^4). \quad (7)$$

This expression shows that all odd-order dispersion terms vanish, thereby demonstrating nonlocal dispersion cancellation. Furthermore, because all beams propagate through the same Sagnac loop, the zeroth-order phase term also cancels naturally. As a result, the interference pattern depends solely on the chromatic dispersion of the fiber under test, which enhances the measurement precision by reducing the number of relevant parameters. This property also underpins the self-referenced nature of the measurement: the relative phase is not defined with respect to an independent reference arm, but arises directly from the interference between the two counter-propagating nonlinear contributions generated within the same loop. Consequently, the extracted dispersion is inherently insensitive to absolute path lengths, global phase offsets, and common-mode environmental fluctuations. Finally, all the light exits the loop via the PBS and is directed to the final port of the circulator. A second PBS then projects the idler interference onto the appropriate polarization basis, and both output ports are recorded on a commercial optical spectrum analyzer (OSA), as shown in Fig. 2. This fully fiber-based readout provides fast, alignment-free chromatic dispersion measurements without the need for active synchronization or narrowband filtering, in contrast to conventional QWLI schemes.

III. DISCUSSION

The probability of detecting an idler photon at the output of the interferometer is given by

$$P_{H,V}(\omega_i) \propto \frac{S(\omega_p, \omega_s, \omega_i)}{2} (1 \pm \mathcal{V} \cos \Phi), \quad (8)$$

where S is the total transmission spectrum of the system, encompassing the DFG spectral acceptance of the nonlinear crystal and the transmission of all optical components. The subscripts H and V denote the horizontal and vertical polarization, respectively, and \mathcal{V} is the fringe visibility.

Because both outputs of the interferometer are measured, the normalized interference pattern reads:

$$P = \frac{P_H - P_V}{P_H + P_V} = \mathcal{V} \cos \Phi. \quad (9)$$

This normalization eliminates the need for prior calibration of the system transmission and suppresses the influence of losses and spectral response. The fringe contrast quantifies the indistinguishability of the two idler contributions in the loop and is governed by the following conditions:

- Polarization alignment along the loop: If the FUT is polarization-maintaining (PM), the loop preserves polarization without further adjustment.

Otherwise, a polarization controller (PC_2 , see Fig. 1.a) is used to match the states in the two arms; in this case, an initial calibration of the CD with PC_2 is required.

- Spectral overlap of the CW and CCW contributions: This condition is inherently satisfied since only one nonlinear crystal is used, ensuring identical nonlinear optical properties in both directions.
- Balance of idler spectral amplitudes: Losses in the FUT or asymmetric coupling at the crystal pigtails can introduce imbalance. This can be compensated for by adjusting the input pump and signal power ratio with PC_1 (see Fig. 1.a).

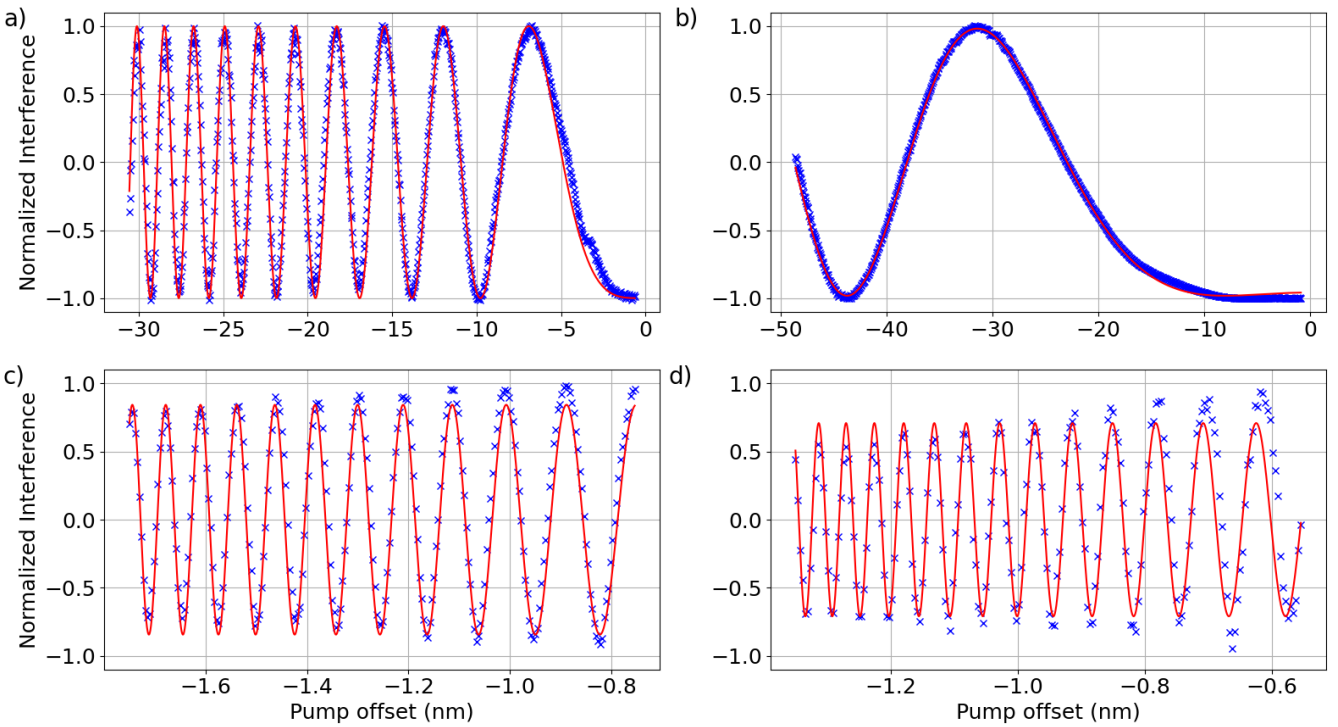


FIG. 3. Normalized interference patterns (experimental data, blue) and corresponding fits (red) using Eq. (9). The results are shown for (a) a 1m long PM dispersion-compensating fiber, (b) a 25cm long PM fiber, (c) a dispersion-compensation fiber module of $L \approx 200$ m, and (d) a $L \approx 4$ km coil of standard telecom single-mode fiber. These measurements illustrate the versatility of the method, covering dispersion-length products from sub-meter to multi-kilometer scale.

Two additional considerations are critical for optimizing CD measurements. First, the residual background noise originating from the pump and signal beams in the idler detection band must be properly evaluated. This noise differs depending on the output port owing to the intrinsic phase stability of the loop. Second, care must be taken to prevent the SLED from producing second-harmonic light. If so, the energy and phase conservation conditions for the idler would no longer reference a fixed frequency, thereby invalidating the odd-order dispersion cancellation. In our case, the full width at half maximum

(FWHM) of the crystal's SHG acceptance bandwidth is narrower than the WDM bandwidth used to combine the pump and signal, effectively preventing unwanted SHG.

The first CD measurement, shown in Fig. 3 (a) was performed with a 1 m long PM dispersion-compensating fiber. Fitting the normalized interference pattern with Eq. (9) yields a CD value of $8.200 \times 10^{-2} \pm 3 \times 10^{-5}$ ps/nm, which is among the most precise interferometric CD measurements reported to date [9, 16, 20]. The high fringe visibility ($\mathcal{V} \approx 95\%$) confirms the validity of the protocol. The residual CD measurement, i.e. with

no fiber under test, does not exhibit interference fringes over the entire spectral range.

To demonstrate the versatility of the method, we extended the measurement to three additional samples: (i) a 25cm long PM fiber, (ii) a fiber-based dispersion compensation module of length $L \approx 200$ m and (iii) a fiber coil of ≈ 4 km. The corresponding normalized spectra and fits are shown in Fig. 3, yielding CD values of $4.128 \times 10^{-3} \pm 3 \times 10^{-6}$ ps/nm, $35.97 \pm 1 \times 10^{-2}$ ps/nm and $72.95 \pm 4 \times 10^{-2}$ ps/nm, respectively. For longer samples (Fig. 3 (c) and (d)), the fringe visibility decreases slightly as the measurement deviates from the pump frequency. This effect arises from the narrowing fringe period approaching the resolution limit of the OSA, $\Delta\lambda = 4$ pm. From this limitation, we estimate that the setup can resolve fringes for CD values up to 170 ps/nm, equivalent to ≈ 10 km of standard single-mode telecom fiber. Conversely, for short-length dispersion products, the minimum measurable CD depends on the criterion adopted for resolving interference fringes. If we consider the conservative requirement of observing at least one full fringe, its spectral width is

$$\Delta\lambda = \left(\frac{\lambda_p^4}{2\pi c^2 |\beta^{(2)}| L} \right)^{1/2}. \quad (10)$$

Using $\Delta\lambda \approx 90$ nm, corresponding to the FWHM of the crystal's DFG acceptance, this criterion yields a minimum resolvable CD of $\approx 10^{-3}$ ps/nm, which is equivalent to approximately 6 cm of standard single-mode telecom fibre. Such sensitivity makes the setup particularly relevant for characterizing very short devices, including integrated waveguides and nonlinear components, where dispersion plays a critical role. This minimum value can be further reduced by employing a shorter nonlinear crystal, which increases the DFG acceptance bandwidth.

Although the ultimate sensitivity of our experiment is bounded by the standard quantum limit, the proposed scheme removes many of the practical limitations encountered in previous interferometric approaches. Linear interferometers require passive or active stabilisation of the relative phase, which increases complexity and can restrict the accessible sample length. SU(1,1) nonlinear interferometers offer intrinsic phase sensitivity but impose strict constraints: the sample under test must be transparent to both pump and signal wavelengths, and the losses directly degrade the fringe visibility. In contrast, in our configuration, the pump analogue at frequency $2\omega_p$ is confined within the nonlinear crystal, so that only telecom-band light circulates in the loop, and the visibility can be restored by tuning the input state polarization. Quantum two-photon approaches further require spectral or time-domain filtering and single-photon detection, leading to long acquisition times and higher system complexity, whereas our method relies solely on bright classical fields and standard spectral detection. In

addition, our architecture operates without coherence-time restrictions on the pump laser relative to the sample length, unlike many conventional schemes. Altogether, the combination of self-stabilization and self-referencing, full telecom compatibility, robustness to loss, and simple broadband readout makes our approach a practical and versatile alternative to existing interferometric techniques for chromatic dispersion measurements.

IV. CONCLUSION

We have presented a new interferometric method for chromatic dispersion measurement based on a cascaded nonlinear Sagnac loop. By exploiting energy and phase conservation in the nonlinear process, the interference spectrum becomes dependent only on the chromatic dispersion of the sample, with the zeroth-order and all odd-order dispersion terms intrinsically cancelled. This allowed us to obtain high-contrast, calibration-free interference fringes using standard telecom components, achieving state-of-the-art precision. We further demonstrated the versatility of the method by characterizing samples ranging from tens of centimeters to several kilometers, showing that both small and large dispersion-length products can be accessed within the same platform. The combination of self-referencing, full telecom compatibility, broadband acceptance, and rapid acquisition makes this technique a practical and scalable solution for chromatic dispersion metrology in both laboratory and industrial environments.

ACKNOWLEDGMENT

This work was conducted within the framework of the OPTIMAL project, granted by the European Union through the Fond Européen de développement régional (FEDER). The authors also acknowledge financial support from the Agence Nationale de la Recherche (ANR) through the projects METROPOLIS (ANR-19-CE47-0008), QAFEINE (21-ASTR-0007-DA), and PARADIS (ANR-22-ASTR-0027-01).

AUTHOR INFORMATION

All authors contributed equally to the entire process, from the first draft to the final version of the manuscript before submission. All authors have read, discussed, and contributed to the writing, reviewing, and editing of the manuscript.

COMPETING INTERESTS

The authors declare no conflict of interest.

DATA AVAILABILITY

The data are available from the authors upon reasonable request.

[1] Abbott, B. Observation of Gravitational Waves from a Binary Black Hole Merger. *Phys. Rev. Lett.* **116**, 061102 (2016,2), <https://link.aps.org/doi/10.1103/PhysRevLett.116.061102>

[2] Huang, D., Swanson, E., Lin, C., Schuman, J., Stinson, W., Chang, W., Hee, M., Flotte, T., Gregory, K., Puliafito, C. & James G. Fujimoto Optical Coherence Tomography. *Science* **254**, 1178-1181 (1991), <https://www.science.org/doi/abs/10.1126/science.1957169>

[3] Xu, Z. & Herman, P. Phase-sensitive interferometry for absolute optical path length measurement: review and applications. *Opt. Lasers Eng.* **51**, 1015-1022 (2013)

[4] Fink, M., Steinlechner, F., Handsteiner, J., Dowling, J., Scheidl, T. & Ursin, R. Entanglement-enhanced optical gyroscope. *New Journal Of Physics* **21**, 053010 (2019,5), <https://dx.doi.org/10.1088/1367-2630/ab1bb2>

[5] Dalidet, R., Martin, A., Riesner, M., Ahmedou, S., Dauliat, R., Leconte, B., Walter, G., Sauder, G., Delagnes, J., Millot, G., Roy, P., Jamier, R., Tanzilli, S. & Labonté, L. Plug-and-Play Measurement of Chromatic Dispersion by Means of Two-Photon Interferometry. *Phys. Rev. Appl.* **20**, 024026 (2023,8), <https://link.aps.org/doi/10.1103/PhysRevApplied.20.024026>

[6] Baker, C., Lu, Y. & Bao, X. Chromatic-dispersion measurement by modulation phase-shift method using a Kerr phase-interrogator. *Opt. Express* **22**, 22314-22319 (2014,9), <https://opg.optica.org/oe/abstract.cfm?URI=oe-22-19-22314>

[7] Bogaerts, W., De Heyn, P., Van Vaerenbergh, T., De Vos, K., Kumar Selvaraja, S., Claeys, T., Dumon, P., Bienstman, P., Van Thourhout, D. & Baets, R. Silicon microring resonators. *Laser & Photonics Reviews* **6**, 47-73 (2012,1)

[8] Abedin, K., Hyodo, M. & Onodera, N. Measurement of the chromatic dispersion of an optical fiber by use of a Sagnac interferometer employing asymmetric modulation. *Opt. Lett.* **25**, 299-301 (2000,3), <https://opg.optica.org/ol/abstract.cfm?URI=ol-25-5-299>

[9] Kaiser, F., Vergyris, P., Aktas, D., Babin, C., Labonté, L. & Tanzilli, S. Quantum enhancement of accuracy and precision in optical interferometry. *Light: Science & Applications* **7**, 17163-17163 (2018,3,1), <https://doi.org/10.1038/lsa.2017.163>

[10] Huelist, F., Kong, J., Liu, C., Jing, J., Ou, Z. & Zhang, W. Quantum metrology with parametric amplifier-based photon correlation interferometers. *Nat Commun.* **5**, 3049 (2014,1), <https://www.nature.com/articles/ncomms4049>

[11] Chekhova, M. & Ou, Z. Nonlinear interferometers in quantum optics. *Advances In Optics And Photonics* **8**, 104 (2016,3), <https://www.osapublishing.org/abstract.cfm?URI=aop-8-1-104>

[12] Kalashnikov, D., Paterova, A., Kulik, S. & Krivitsky, L. Infrared spectroscopy with visible light. *Nature Photonics* **10**, 98-101 (2016,2,1), <https://doi.org/10.1038/nphoton.2015.252>

[13] Lemos, G., Borish, V., Cole, G., Ramelow, S., Lapkiewicz, R. & Zeilinger, A. Quantum imaging with undetected photons. *Nature* **512**, 409-412 (2014,8,1), <https://doi.org/10.1038/nature13586>

[14] Paterova, A., Yang, H., An, C., Kalashnikov, D. & Krivitsky, L. Measurement of infrared optical constants with visible photons. *New Journal Of Physics* **20**, 043015 (2018,4), <https://dx.doi.org/10.1088/1367-2630/aab5ce>

[15] Riazi, A., Zhu, E., Chen, C., Gladyshev, A., Kazansky, P. & Qian, L. Alignment-free dispersion measurement with interfering biphotons. *Opt. Lett.* **44**, 1484-1487 (2019,3), <https://opg.optica.org/ol/abstract.cfm?URI=ol-44-6-1484>

[16] Riazi, A., Chen, C., Zhu, E., Gladyshev, A., Kazansky, P., Sipe, J. & Qian, L. Dispersion measurement assisted by a stimulated parametric process. *Opt. Lett.* **45**, 2034-2037 (2020,4), <https://opg.optica.org/ol/abstract.cfm?URI=ol-45-7-2034>

[17] Franson, J. Nonlocal cancellation of dispersion. *Phys. Rev. A* **45**, 3126-3132 (1992,3), <https://link.aps.org/doi/10.1103/PhysRevA.45.3126>

[18] Kim, T., Fiorentino, M. & Wong, F. Phase-stable source of polarization-entangled photons using a polarization Sagnac interferometer. *Phys. Rev. A* **73**, 012316 (2006,1), <https://link.aps.org/doi/10.1103/PhysRevA.73.012316>

[19] Dalidet, R., Martin, A., Sauder, G., Labonté, L. & Tanzilli, S. Quantum-like nonlinear interferometry with frequency-engineered classical light. *Scientific Reports* **15**, 27654 (2025,7,29), <https://doi.org/10.1038/s41598-025-09533-7>

[20] Dalidet, R., Martin, A., Riesner, M., Ahmedou, S., Dauliat, R., Leconte, B., Walter, G., Sauder, G., Delagnes, J., Millot, G., Roy, P., Jamier, R., Tanzilli, S. & Labonté, L. Plug-and-Play Measurement of Chromatic Dispersion by Means of Two-Photon Interferometry. *Phys. Rev. Appl.* **20**, 024026 (2023,8), <https://link.aps.org/doi/10.1103/PhysRevApplied.20.024026>